

## ARTICLE



# Lipid nanoparticle mediated base editing of the Q344X rhodopsin mutation associated with retinitis pigmentosa

Victoria A. C. Palmgren<sup>1</sup>, Miffy Hok Yan Cheng<sup>2</sup>, Yao Zhang<sup>1,3,4</sup>, Tiffany Carlaw<sup>2,3</sup>, Tessa Morin<sup>2</sup>, Jerry Leung<sup>1</sup>, Colin JD Ross<sup>2</sup>, Pieter R. Cullis<sup>1</sup> and Robert S. Molday<sup>1</sup>✉

© The Author(s), under exclusive licence to Springer Nature Limited 2025

Retinitis pigmentosa (RP) associated with mutations in the rhodopsin gene (*RHO*) is a significant cause of blindness. Here we report on the application of adenine base editing of the c.1030C>T (p.Q344X) *RHO* mutation linked to RP. Using a fluorescence reporter cell system, we optimized editing by exploring base editors, sgRNA, and delivery methods. Flow cytometry, western blotting, and immunofluorescence microscopy confirmed the restoration of full-length rhodopsin after editing. DNA sequencing verified editing at the target nucleotide and the absence of bystander edits within the editing window. Polyethylenimine cationic polymer transfection of cells with a plasmid containing the NG-ABE8e adenine base editor and A6 guide RNA that placed the targeted adenine in position 6 of the editing window resulted in 31.0% gDNA sequence correction and 26.3% rhodopsin protein correction as determined by flow cytometry. Purified NG-ABE8e protein complexed with A6-sgRNA showed 32.2% gDNA editing and 44.5% rhodopsin correction. Plasmid NG-ABE8e and A6-sgRNA co-encapsulated into lipid nanoparticles (LNPs) and transfected into the reporter cell system resulted in the highest editing (42.6% gDNA editing and 65.9% rhodopsin correction). These results demonstrate the successful correction of the c.1030C>T *RHO* mutation and provide the foundation for base editing as a treatment for RP.

*Gene Therapy*; <https://doi.org/10.1038/s41434-025-00584-z>

## INTRODUCTION

Inherited retinal diseases (IRD) are a heterogeneous group of disorders that constitute a significant cause of visual impairment affecting over five million people worldwide [1]. They are typically characterized by progressive vision loss caused by mutations in genes encoding proteins essential for the function and/or survival of photoreceptor cells. Currently, there is only one genetic treatment for patients suffering from IRDs. Luxturna (voretigene neparvovec) is an adeno-associated virus (AAV) based gene augmentation therapy for Leber Congenital Amaurosis-2 (LCA2). This treatment provides retinal pigment epithelial (RPE) cells expressing a defective RPE65 gene with a functional copy of the gene through a one-time subretinal injection [2–4]. While AAV-mediated gene augmentation has been life-altering for individuals with LCA2, its overall application for IRDs is still limited.

As opposed to gene augmentation, CRISPR-mediated gene editing has emerged as a strong candidate for the treatment of IRDs [5]. Base editing, developed from CRISPR-Cas9, utilizes deaminases to directly perform single-nucleotide conversions. This mechanism is irreversible, specific, and has fewer off-target effects than traditional CRISPR and, therefore, is more suitable for therapeutic intervention. Previously, Choi et al. used subretinal injections of a lentivirus targeting a nonsense mutation in the *RPE65* gene in a mouse model for LCA2 [6]. They found 40% correction efficiency and preserved cone photoreceptor

transduction and survival. Using dual AAV encoding a split intein base editor to correct a mutation in *ABCA4*, one study achieved a high average editing of 87% in RPE cells and 75% in cones in non-human primates and mice [7]. Another study investigated base editing paired with AAV delivery for correcting the *phosphodiesterase 6b* (*Pde6b*) gene in photoreceptors of a mouse model for retinitis pigmentosa (RP) [8]. They found 37% editing efficacy, which correlated with preservation of photoreceptors and rescue of visual function. Together, these studies highlight the versatility of gene editing for the application of ocular diseases. While viral delivery methods are being widely employed for the delivery of both gene augmentation and gene editing, increasing attention is being directed to alternative delivery methods.

Lipid nanoparticles (LNPs) are an attractive alternative to AAV because of their ability to encapsulate a wide variety of biomolecules, minimal immunogenicity, ease of customization, and substantially lower manufacturing cost. However, despite their advantages, effective delivery to target ocular tissues presents unique challenges. LNP delivery to retinal cells via intravitreal injection is hindered by the inner limiting membrane [9]. Conventional LNP formulation, delivered by subretinal injection, leads to expression of cargo primarily in the RPE cells [10]. To date, however, there have been limited studies on LNP delivery directly to photoreceptor cells. To facilitate expression, recent studies have looked at modifying the surface of the LNP

<sup>1</sup>Department of Biochemistry and Molecular Biology, University of British Columbia, Vancouver, BC, Canada. <sup>2</sup>Faculty of Pharmaceutical Sciences, University of British Columbia, Vancouver, BC, Canada. <sup>3</sup>School of Biomedical Engineering, University of British Columbia, Vancouver, BC, Canada. <sup>4</sup>Michael Smith Laboratories, University of British Columbia, Vancouver, BC, Canada. ✉email: robert.molday@ubc.ca

Received: 28 April 2025 Revised: 11 September 2025 Accepted: 25 November 2025

Published online: 10 December 2025

either by altering the type of PEG-lipid [11] or adding targeting peptides [12]. Altering the formulation method has also been shown to alter the targeting of the LNP in the retina [13]. While promising, the delivery of functional gene editing technology has yet to be shown.

Here we report on the development of an in vitro reporter system for optimizing base editing and its application to the editing of the c.1030C>T (p.Q344X) nonsense mutation in the rhodopsin (*RHO*) gene. Rhodopsin is a G-protein coupled receptor present in rod outer segment disk membranes and is responsible for the initiation of the phototransduction cascade [14, 15]. This Q344X mutation prevents the translation of the VxPx localization signal, which leads to mislocalization of the rhodopsin to the inner segment [16–18]. Characterized as autosomal dominant RP, this mutation in *RHO* leads to photoreceptor degeneration and ultimately vision loss. Base editing of rhodopsin has been performed using a split-intein dual-AAV to deliver an adenine base editor (ABE). They found an average of 18.2% correction, which correlated with sustained rhodopsin expression in p15 mice, but which did not produce a phenotypic rescue [19]. The abundance of mutations that are targetable by base editing is highlighted in a study that determined 55% of *RHO*-variants could be corrected with base editors [20]. Here, we describe the development and application of a reporter system that enables systematic screening and quantitative evaluation of optimal base editing strategies. Using this system, we show that an ABE encapsulated in LNPs achieved high editing efficiency, highlighting the therapeutic potential of ABE-LNP delivery for the correction of the Rho Q344X mutation. These results highlight the importance of optimizing both the base editor system and its delivery, including the choice between DNA or Ribonucleoprotein (RNP) modalities. Although this study focuses on the editing of the Q344X mutation in rhodopsin, the in vitro reporter system developed here is widely applicable for the optimization of base and prime editing of genes associated with other genetic diseases.

## MATERIAL AND METHODS

### Cell culture

Flp-In™-293 cell line (Thermo Fisher, Waltham, MA, USA (catalog # R750-07)) was maintained in Dulbecco's Modified Eagle Medium (DMEM) (Sigma-Aldrich) supplemented with 10% fetal bovine serum (Thermo Fisher Scientific), 1% penicillin/streptomycin (Thermo Fisher Scientific), 1% L-glutamine (Thermo Fisher Scientific), and 100 µg/ml zeocin (Thermo Fisher Scientific). Stable cell lines expressing wild-type (WT) or Q344X rhodopsin were generated using the Flp-In System according to the manufacturer's protocol. Following transfection, the medium was replaced with complete DMEM supplemented with 100 µg/ml hygromycin B. Hygromycin-resistant foci were isolated, expanded, and then analyzed for expression of the gene of interest and enhanced green fluorescent protein (EGFP). Sanger sequencing was used to confirm stable cell genotypes.

### Plasmid subcloning and base editor transfection

EGFP was excised from the pCAG-EGFP vector (Addgene #11150) and cloned into pcDNA5/FRT using the Xma1 and Xho1 restriction sites. Murine rhodopsin cDNA was PCR amplified to remove the stop codon and add Not1 and Xma1 restriction sites and cloned into the EGFP-pcDNA5/FRT plasmid. Q344X (c.1030C>T) rhodopsin was generated by PCR-based site-directed mutagenesis. Primers are listed in Supplementary Table S1. Base editor plasmids were obtained from Addgene (NG-ABE8e (#138491), ABE8e (#138489), NG-ABEmax (#124163), xCas9(3.7)-ABE7.10 (#108382), ABE9 (#194208)). ABE9-SPRY was generated in-house. Modified synthetic sgRNAs—containing 2'-O-methyl analogs first and last 3 bases; 3' phosphorothioate between first 3 and last 2 bases, and an 80-nucleotide scaffold that contains the binding site for spCas 9—were purchased from Synthego. sgRNA sequences are listed in Supplementary Table S2.

For cationic polymer delivery of plasmid ABE, reporter cells were transfected with 1.25 µg of sgRNA and ABE plasmid (4:1 (w/w) ratio) for each  $1 \times 10^6$  cells with 3.25 µg of linear polyethylenimine hydrochloride

(PEI) (Polysciences Inc., Warrington, PA, USA; catalog # 24765, MW 40,000). Analyses were conducted 48 h post-transfection.

### Flow cytometry

Reporter cells were dissociated with 0.5% trypsin-EDTA, resuspended in PBS with 0.1 M EDTA, and stained with 0.01 µM Calcein Violet-AM (Biolegends, San Diego, CA, USA (Catalog# 425203)) for exclusion of nonviable cells. Samples were measured on an Attune NxT flow cytometer (ThermoFisher Scientific). Flow cytometry results were analyzed with FlowJo software (v10.10.0). The data was analyzed using Prism 9 (GraphPad Software) and expressed as mean ± SEM. Percent editing was presented as the % EGFP+ edited cells after subtracting the unedited control, and normalized to WT cells.

### SDS gel electrophoresis and western blotting

Reporter cells were harvested, washed, and pelleted at  $1500 \times g$  (Eppendorf Centrifuge 5424) in PBS. The final pellet was resuspended in 75 µl of resuspension buffer (50 mM HEPES, 150 mM NaCl, 4 mM MgCl<sub>2</sub>, 1 mM dithiothreitol (DTT), 1× protease inhibitor cocktail (Millipore Sigma 539134), 10% glycerol) and added to 150 µl of solubilization buffer (resuspension buffer + 18 mM CHAPS). After 1 h of stirring at 4 °C, the solution was centrifuged at  $40,000 \times g$  (TLA 55 rotor, Beckman Coulter) for 12 min, and the supernatant was retained for SDS gel electrophoresis. To facilitate the quantification of full-length rhodopsin in samples subjected to base editing, deglycosylation of the cell lysate was carried out at 32 °C using PNGase F (New England Biolabs, Ipswich, MA, catalog #P07045) according to the manufacturer's instructions.

Samples were separated on an 11.5% SDS-PAGE gel. Western blots were labeled with a primary antibody followed by a secondary antibody for visualization on an Odyssey Li-Cor system as previously described [21]. Antibodies are listed in Supplementary Table S3. Uncropped gel images can be found in the Supplementary Figs. S1, S2. BLUeye Prestained Protein ladder (Froggabio) was loaded as a molecular weight marker. Relative protein expression was quantified by densitometry of the western blotting band normalized to a loading control (ezrin) using Li-Cor Image Studio (v 6.0.0.28). Data was then analyzed using Prism 9 (GraphPad Software).

### Immunofluorescence microscopy

Coverslips were coated for 1 h with 0.02 mg/ml poly-L-lysine (ThermoFisher).  $0.5 \times 10^6$  reporter cells plated on coverslips were transfected as above. After 48 h, cells were fixed in 4% paraformaldehyde/0.1M phosphate buffer (PB), pH 7.2, for 30 min and washed with PB 3× for 15 min each. Cells were blocked and permeabilized with 10% normal goat serum (NGS) and 0.2% Triton X-100 in PB for 30 min and subsequently labeled with primary, followed by secondary antibodies as previously described [22]. Antibodies listed in Supplementary Table S3 were diluted in PB containing 0.3% NGS/0.1% Triton X-100. DAPI (4',6-diamidino-2-phenylindole) at 1:2000 dilution was used as a nuclear marker. Fluorescence was detected using a Zeiss LSM700 confocal microscope (Carl Zeiss, Oberkochen, Germany). Images were analyzed using ZEN Microscopy software and Fiji (ImageJ v2.3.0/1.53f).

### Genomic DNA sequencing-PCR and primers

Genomic DNA (gDNA) was extracted in lysis buffer (10 mM Tris-HCl, pH 7.0, 0.05% SDS, 25 µg/ml Proteinase K (New England Biolabs P8107S)). The gDNA mixture was incubated at 37 °C for 1 h, followed by 20 min at 80 °C. PCR using Phusion® polymerase (New England Biolabs) was performed according to the manufacturer's protocol; reaction conditions are listed in Supplementary Table S4. Targeted next-generation amplicon sequencing was used for editing detection. Amplified segments of gDNA within the target region were sequenced using Amplicon-EZ sequencing from Genewiz/Azenta Biosciences. NGS reads were analyzed using CRISpresso2 [23]. The primers used for amplification are listed in Supplementary Table S1.

### LNP generation and transfection

LNPs were formulated with a lipid mixture of heptatriaconta-6,9,28,31-tetraen-19-yl 4-(dimethylamino)butanoate (DLin-MC3-DMA; MC3), 1,2-distearoyl-sn-glycero-3-phosphorylcholine (DSPC), cholesterol, and (R)-2,3-bis(octadecyloxy)propyl-1-(methoxy polyethylene glycol 2000) carbamate (PEG-DMG<sub>2k</sub>) at a ratio of 50/10/38.5/1.5 mol%, respectively, using previously established procedures [24, 25]. Briefly, LNPs were prepared by injecting 10 mM total lipid composition in anhydrous ethanol with an

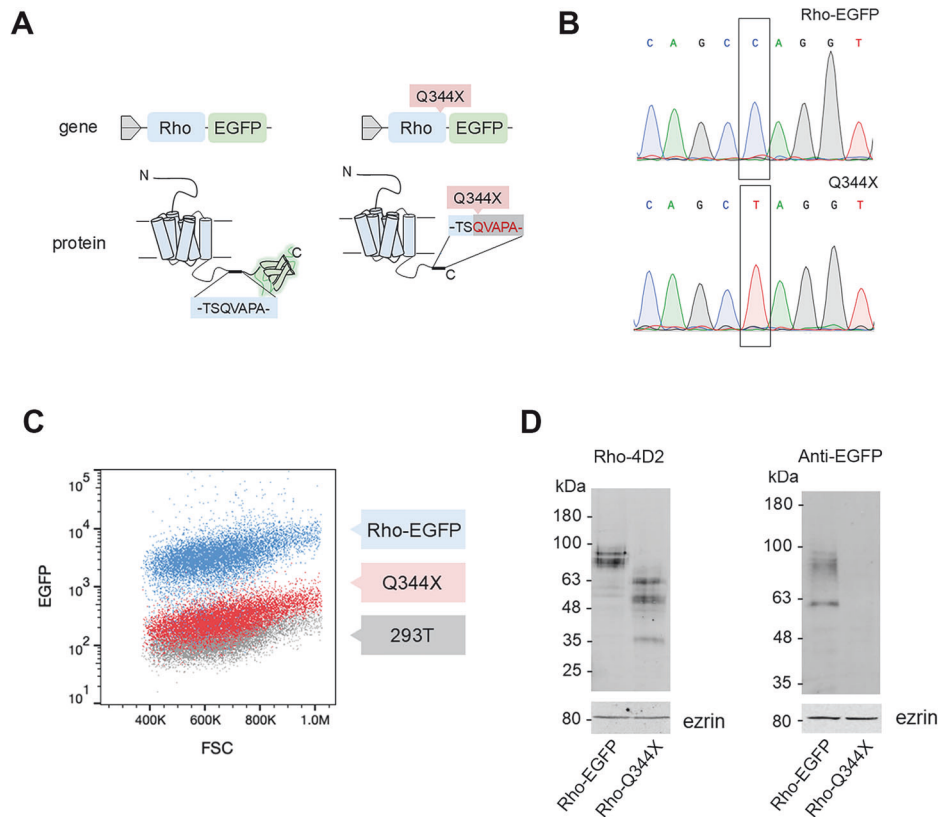


**Fig. 1 Validation of Rho-EGFP and Rho-Q344X-EGFP stable cell lines.** **A** A schematic diagram of the reporter construct, Rho and Rho-Q344X tagged on the C-terminus with EGFP. In the Q344X model, the QVAPA localization signal is not translated. **B** Validation by Sanger sequencing of the c. 1030C>T mutation that causes translation of a premature stop codon at position amino acid 344. **C** Representative flow cytometry dot plots of Rho-EGFP cells, Rho-Q344X-EGFP cells, and untransfected Flp-In 293T Host cells. Results were quantified per 100,000 cells. **D** Representative western blots labeled for rhodopsin with the Rho-4D2 monoclonal antibody and EGFP with an anti-EGFP antibody. The N-terminal Rho-4D2 antibody labels both Rho-EGFP and Rho-Q344X; the anti-EGFP antibody only labels Rho-EGFP. Multiple bands are due to heterogeneous glycosylation of rhodopsin expressed in culture 293T cells. Ezrin was used as a loading control. EGFP enhanced green fluorescence protein, FSC forward scattering.

aqueous phase containing plasmid ABE and sgRNA (1:3 (w/w ratio) dissolved in 300 mM Na-citrate (pH 4) through a T-junction with a 3:1 aqueous:ethanol ratio (v/v) with an amine-to-phosphate ratio [N/P] of 6. Lipids were purchased from Avanti Polar Lipids (Alabaster, AL) except cholesterol, which was purchased from Sigma Aldrich (St. Louis, MO). Flow rates were 5 ml/min for the ethanolic lipid phase and 15 ml/min for the aqueous RNA (or DNA) phase for a total output flow rate of 20 ml/min. The resulting formulations were then dialyzed in Spectra/Por 2 dialysis tubing with a 12–14 kD MWCO (Repligen, Waltham, MA, USA) against 1000-fold volumes of phosphate-buffered saline (pH 7.4) over a period of 16 h at room temperature. Formulations were then concentrated by centrifugation at  $1500\times g$  in Amicon Ultra-15 Centrifugal Filter Units (MilliporeSigma, Burlington, MA, USA). Particle size and polydispersity index (PDI) were measured as the number mean average, determined via dynamic light scattering using the Malvern Zetasizer Nano ZS. The encapsulation efficiency of the cargo was quantified using the Quant-iT RiboGreen RNA Assay Kit (Wako Diagnostics, Mountain View, CA, USA). The particles were then aliquoted and frozen with 5% sucrose at  $-80^{\circ}\text{C}$ . Cryo-EM imaging was performed as previously described [25]. Low-magnification cryo-EM images can be found in Supplementary Fig. S3. For transfections, reporter cells were seeded at  $1\times 10^6$  cells in a 6-well plate.  $1\ \mu\text{g}$  of LNP was added to the cell culture media, and cells were harvested for subsequent analysis after 48 h.

#### Ribonucleoprotein expression and purification and delivery

NG-ABE8e in a bacterial protein expression plasmid [26] was expressed in BL21 cells and purified on a Ni-NTA affinity column, followed by cation exchange chromatography as described [5]. The purified NG-ABE8e was confirmed by SDS-Page (Supplementary Fig. S4), quantified by nanodrop, flash-frozen in liquid nitrogen, and stored in  $-80^{\circ}\text{C}$ . Reporter cells at

$1\times 10^6$  cells were transfected with RNP (6250 ng NG-ABE8e protein, 1200 ng sgRNA using Lipofectamine CRISPRmax according to the manufacturer's protocol (ThermoFisher).

#### Statistical analysis

All experiments were performed multiple times, with the number of repetitions indicated in the figure caption, and in data shown in relevant figures. Means  $\pm$  standard error of the mean (SEM) are presented. Significant differences reported in figures were identified using an unpaired *t*-test unless otherwise indicated in the figure captions. Statistical significance was set as  $*p < 0.05$ ,  $**p < 0.01$ ,  $***p < 0.001$ , and  $****p < 0.0001$ , with a 95% confidence interval. Statistical analysis and graphing was done using GraphPad Prism software (v9 GraphPad Software, Boston, MA, USA).

## RESULTS

### EGFP reporter system for base editing

We developed a fluorescence reporter system in which EGFP was fused to the C-terminus of rhodopsin to generate WT rhodopsin (Rho-EGFP) or the rhodopsin variant (Rho-Q344X) (Fig. 1A). The latter contains a single nucleotide substitution (c.1030C>T) that results in premature termination of translation. This truncation results in the loss of the localization signal VxPx, which in photoreceptors causes mislocalization of rhodopsin [16]. In our HEK293 cell model, this mutation prevents the expression of EGFP (Fig. 1A). The integration of the *RHO-EGFP* gene into the stable cell line was confirmed by Sanger sequencing of gDNA (Fig. 1B)

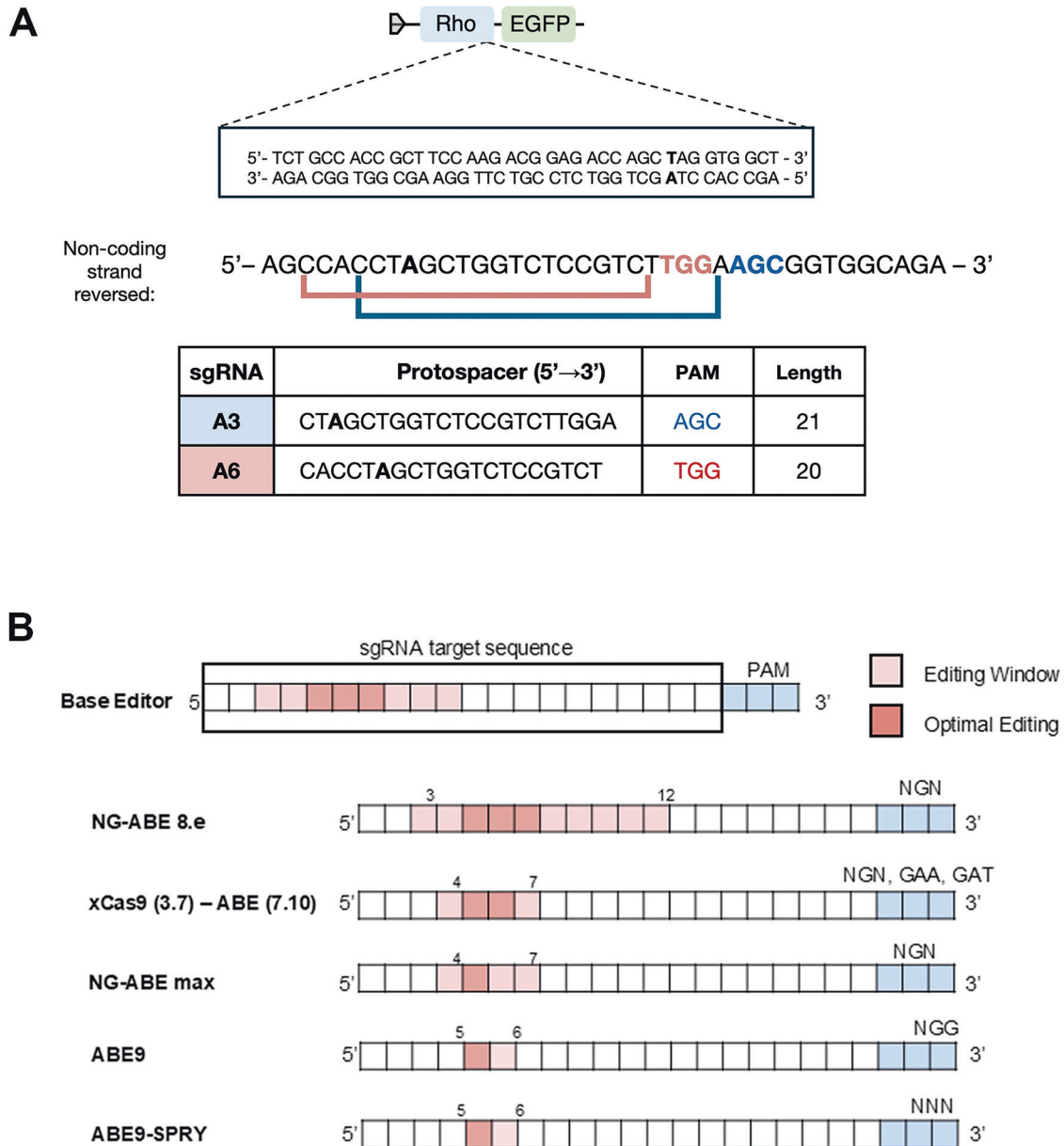


**Fig. 2 Base editor selection and sgRNA design for the Rho-Q344X-EGFP mutant.** **A** The Rho-Q344X-EGFP model has a c.1030C>T (p.Q344X) nonsense mutation. Based on the editing window of this mutation, two sgRNAs were designed to place the target mutation (bold letter) within the ABE activity window. **B** NG-ABE8e, xCas9(3.7)- ABE 7.10, and NG-ABEmax, ABE9, and ABE9-SPRY are the base editors that have been selected based on their editing windows and the protospacer adjacent motif (PAM) that they recognize.

Flow cytometry confirms the expression of the Rho-EGFP fusion protein and the lack of EGFP expression in the rhodopsin variant (Fig. 1C). Validation of the RhoQ344X truncation was confirmed by western blotting (Fig. 1D). The N-terminal Rho4D2 antibody [27] labeled the Rho-EGFP protein and the truncated RhoQ344X variant, whereas the anti-EGFP antibody labeled only the WT protein. The diffuse banding pattern is characteristic of rhodopsin expression in cultured cells and represents heterogeneous N-linked glycosylation [28].

#### PEI transfection of Rho-Q344X-EGFP cells with adenine base editors

To evaluate base editing efficiency *in vitro*, we designed two sgRNAs (A3-sgRNA and A6-sgRNA) with NG and NGG PAM sites, respectively (Fig. 2A). Based on the available PAMs, we selected five ABEs (NG-ABE8e, NG-ABEmax, xCas9(3.7)-ABE(7.10), ABE9,

ABE9-SPRY) most suitable for the window and protospacer position (Fig. 2B). Combinations of ABE and sgRNA were transfected into RhoQ344X cells using PEI as a transfection agent to screen for the ABE/sgRNA combination that produces the highest editing efficiency. A scrambled sgRNA (scr-sgRNA) was used as a negative control. Representative flow cytometry dot plots of RhoQ344X cells transfected with NG-ABE8e and either A3-sgRNA or A6-sgRNA show the highest shift in EGFP cells relative to scr-sgRNA (Fig. 3A). Bar graphs show the percentage of EGFP+ cells for each condition for three biological replicates. A significant increase in EGFP+ cells relative to the scrambled control is observed for NG-ABE8e and A6 sgRNA (A3 6.49%±1.51%, A6 19.95% ±1.42%,  $n = 4$ ), but not for NG-ABEmax, or xCas9(3.7)-ABE(7.10) with either A6 or A3 sgRNA (Fig. 3B).

In a separate experiment, we compared novel base editors using A6-sgRNA, and after transfection with PEI, measured the restoration of the

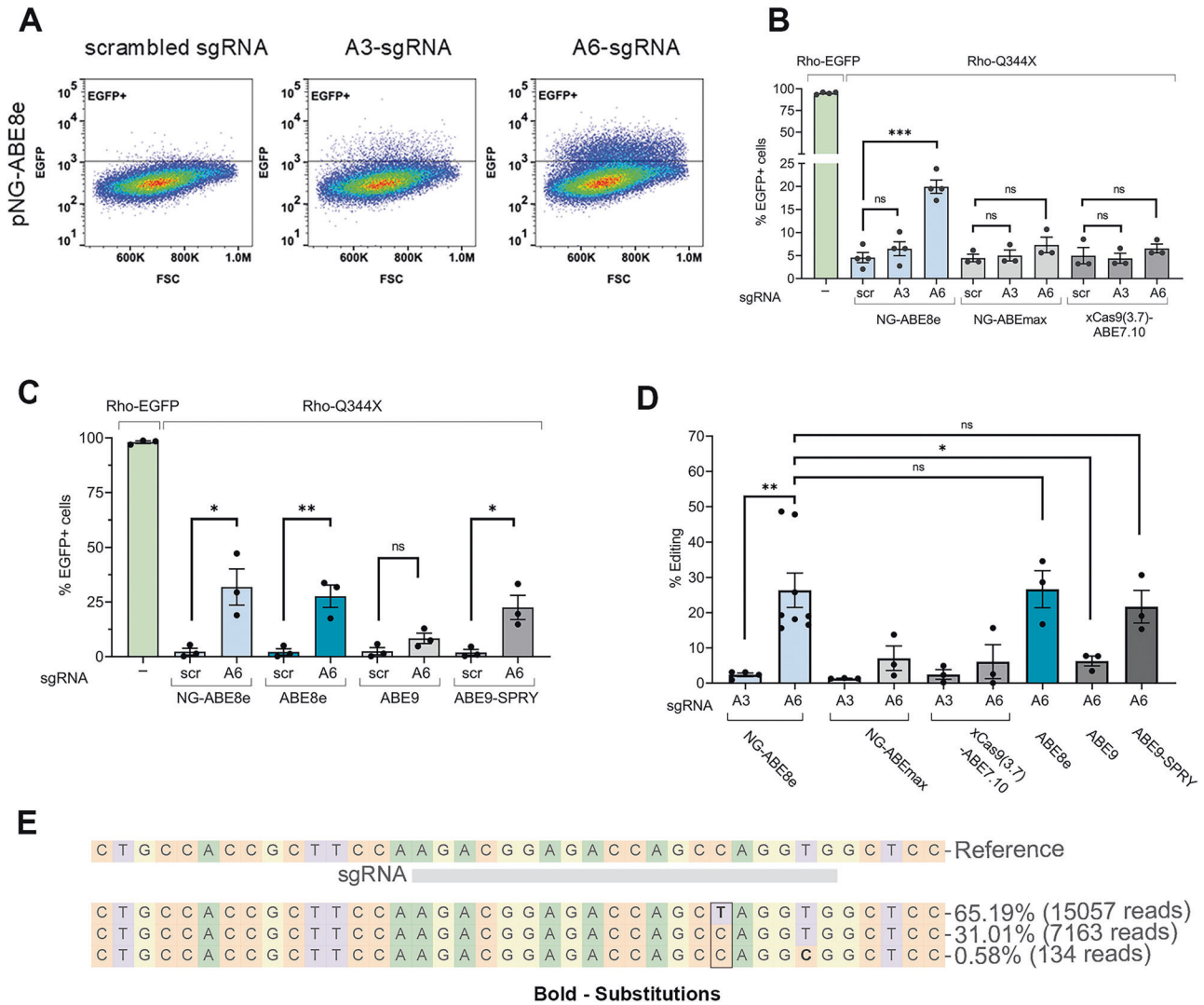


**Fig. 3** Editing of the Rho-Q344X mutation using PEI to transflect plasmid base editors. Stable cells were transfected with PEI with NG-ABE8e, NG-ABEmax, or xCas9(3.7)-ABE7.10 and scrambled (scr) sgRNA negative control, or sgRNA that placed the nucleotide of interest in position A3 or A6 of the editing window.  $1 \times 10^6$  cells were used per condition with 1.25  $\mu$ g of sgRNA and ABE plasmid (4:1 (w/w) ratio) being transfected. Flow cytometry results were quantified per 100,000 cells, with the plots showing the sorting of a population of cells from a single biological replicate. **A** Flow cytometry dot plot showing restoration of the EGFP+ cell population 48 h after transfection. **B** Percent of the cell population that is EGFP+ based on flow cytometry data ( $n = 3$ ,  $\pm$ SEM,  $***p < 0.001$ ). **C** Stable cells were transfected with NG-ABE8e, ABE8e, ABE9, or ABE9-SPRY plasmids and scr sgRNA or A6-sgRNA. 48 h post-transfection, cells were analyzed by flow cytometry, percent of the cell population that is EGFP+ based on flow cytometry data ( $n = 3$ ,  $\pm$ SEM,  $*p < 0.05$ ,  $**p < 0.01$ , ns not significant). **D** Percent editing calculated based on the %EGFP cell population, subtracting the scr sgRNA population and normalizing to the WT population ( $n = 3$ ,  $\pm$ SEM). This data is the average of 3 biological replicates (8 for NG-ABE8e), with 3 technical replicates for each flow cytometry run. **E** Next-generation sequencing results of Q344X transfected with NG-ABE8e and A6 sgRNA. T > C editing is shown in the rectangle.

EGFP signal. NG-ABE8e ( $31.86\% \pm 8.26\%$   $n = 3$ ), ABE8e ( $27.67\% \pm 5.11\%$   $n = 3$ ), and ABE9-SPRY ( $22.54\% \pm 5.55\%$   $n = 3$ ) all had significant restoration levels, with ABE9 being the least efficient ( $8.35\% \pm 2.39\%$   $n = 3$ ) (Fig. 3C). From triple replicates of the flow cytometry data, percent editing was calculated by subtracting the scrambled RhoQ344X control and normalizing to the WT EGFP+ cell population. NG-ABE8e cotransfected with A6-sgRNA had the highest editing at  $24.95 \pm 5.97\%$ . ABE8e-A6 and ABE9-SPRY-A6 had similar levels at  $26.64 \pm 5.26\%$  and  $21.69 \pm 4.62\%$ , respectively. NG-ABEmax, xCas9(3.7)-ABE7.10 and ABE9 all resulted in minimal editing (Fig. 3D). A6 sgRNA was significantly more efficient than A3 sgRNA when used with NG-ABE8e. There was no significant difference when comparing NG-ABE8e to ABE8e or ABE9-SPRY. NG-ABE8e was significantly more efficient than ABE9. gDNA confirmed that 31.01% of the reads were correctly edited (Fig. 3E). WT-RhoEGFP and unedited RhoQ344X gDNA reads were used as controls (Supplementary Fig. S5).

### LNP transfection of Rho-Q344X-EGFP cells with adenine base editor

Comparative studies on cationic polymer transfection and LNP transfection in the retina are limited. However, in vitro, various studies indicate that LNPs transfect cells more efficiently and display a lower level of toxicity than PEI [29–31]. Therefore, we explored LNPs as a method to increase the efficiency of transfection. Plasmid NG-ABE8e was co-encapsulated with A6-sgRNA into LNPs produced based on the Onpattro lipid composition, with modification to the formulation buffer being Na-citrate [25, 32]. NG-ABE8e and A6-sgRNA, which had the highest editing with PEI transfection, was selected to be encapsulated into LNPs for transfection of the reporter cell model. LNP cargo encapsulation efficiency was  $98.02\%$ , size (Z-average) was  $72.23 \pm 1.15$  nm, and polydispersity index was  $0.104 \pm 0.012\%$ . Cryo-EM structure revealed blebs induced by formulation with

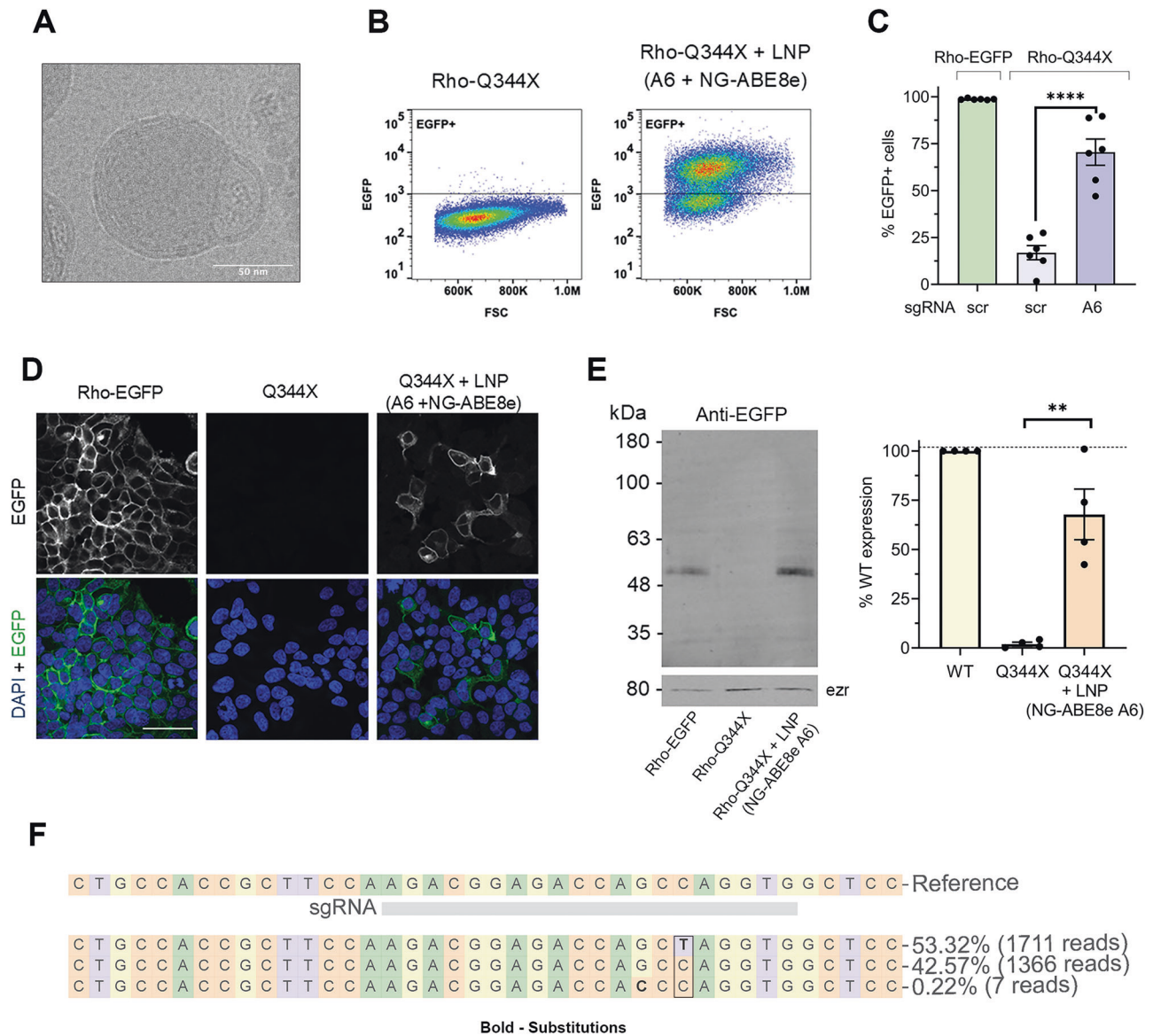


**Fig. 4** Editing of the Rho-Q344X mutation using plasmid ABE encapsulated in LNPs. Stable cells were treated with LNPs encapsulating pNG-ABE8e and either scr-sgRNA or A6-sgRNA (ratio of 1:3). 1 μg LNP (based on DNA/RNA concentration) per  $1 \times 10^6$  cells. **A** Cryo-TEM representative image showing a bleb structure of an LNP containing plasmid DNA (scale bar = 50 nm). **B** Flow cytometry dot plot of representative experiments showing restoration of the EGFP<sup>+</sup> cell population in Q344X mutant cells following transfection. Flow cytometry results were quantified per 100,000 cells, with the plots shown reflecting sorting on a population of cells from a single biological replicate. **C** Percent of the cell population that is EGFP<sup>+</sup> based on flow cytometry data ( $n = 6$ ,  $\pm$ SEM, \*\*\*\* $p < 0.0001$ ). **D** Immunofluorescence microscopy images showing restoration of EGFP expression following treatment with LNP-ABE (scale bar = 50 μm). **E** (Left) Western blot of deglycosylated cell lysate after treatment with LNP using an anti-EGFP antibody. Ezrin (ezr) is used as a loading control. (Right) Quantification of western blots ( $n = 4$ ,  $\pm$ SEM) (\*\* $p < 0.01$  compared to Q344X expression). **F** Next-generation sequencing results of Q344X transfected using LNP with NG-ABE8e and A6 sgRNA. T > C editing is shown in the rectangle.

300 mM Na-citrate buffer (Fig. 4A and Supplementary Fig. S3). Flow cytometry was performed 48 h post-transfection to measure the restoration of the EGFP signal. Representative dot plots for transfection with NG-ABE8e and A6-sgRNA or scr-sgRNA produced a shift in EGFP<sup>+</sup> cells (Fig. 4B). %EGFP<sup>+</sup> cells following LNP transfection showed a significant increase in EGFP restoration ( $70.49\% \pm 7.01\%$   $n = 6$ ) (Fig. 4C). Fluorescence microscopy of EGFP signal further confirms restoration of the EGFP<sup>+</sup> signal following LNP transfection in Rho-Q344X cells (Fig. 4D).

Editing was further analyzed by western blotting. Reporter cells transfected with LNPs containing encapsulated base editor and A6-sgRNA were lysed, the solubilized proteins were subsequently deglycosylated, and western blots were labeled with anti-EGFP

antibody. The results showed a clear restoration of full-length rhodopsin-EGFP (Fig. 4E). This corresponds to  $67.78\% \pm 12.86\%$  in comparison to WT, which is a significant increase compared to the scr control ( $p = 0.0013$ ,  $n = 4$ ). These results confirm the results obtained by flow cytometry. Lastly, gDNA analysis from LNP-A6sgRNA-NG-ABE8e transfected cells showed 42.57% T > C conversion (Fig. 4F).

**Transfection of Rho-Q344X-EGFP cells with ribonucleoprotein**  
The ABE protein, comprised of nCas9 fused with the deaminase, can complex with the sgRNA to form the RNP. Here, we aimed to validate editing efficiency in our reporter model using cationic lipid transfection. After expressing and purifying the Cas9-

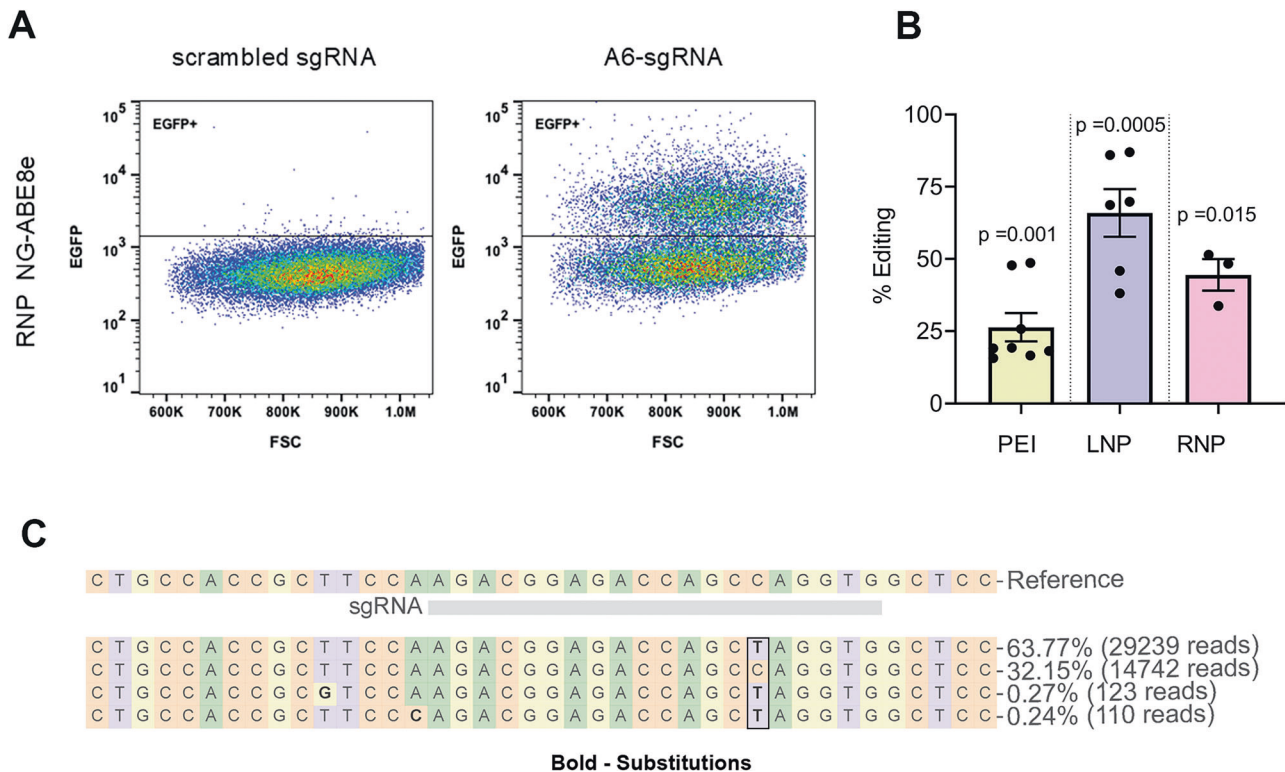


**Fig. 5** Editing of Rho-Q344X mutation using Ribonucleoprotein (RNP). Cas9-deaminase protein (NG-ABE8e) was expressed and purified. After assembly with the sgRNA, the RNP was transfected into the reporter system using Lipofectamine CRISPRmax as a transfection agent. (6.25  $\mu$ g NG-ABE8e protein, 1.2  $\mu$ g sgRNA, per  $1 \times 10^6$  cells). **A** Flow cytometry dot plot of representative experiments showing restoration of the EGFP+ cell population 48 h post-transfection. **B** Percent editing calculated based on the %EGFP cell population, subtracting the scr sgRNA population, and normalizing to the WT population based on flow cytometry data. A 44.49% editing was observed for RNP compared to 26.34% editing with PEI transfection and 65.90% for LNP ( $n = 3$  RNP,  $n = 8$  PEI,  $n = 6$  LNP,  $\pm$ SEM). Significant editing was identified using a one-sample t-test compared to a mean of 0. **C** Next-generation sequencing results of Rho-Q344X transfected with RNP. T > C editing is shown in the rectangle.

deaminase protein (Supplementary Fig. S4), we complexed it to the A6-sgRNA to form an RNP, which was then transfected into the reporter model. Representative flow cytometry dot plots for transfection with RNP NG-ABE8e and A6-sgRNA or scr-sgRNA once again show a shift in EGFP+ cells (Fig. 5A). Based on the flow cytometry data, percent editing was calculated and compared to editing using PEI delivery and LNP delivery of the plasmid ABE (Fig. 5B). LNP delivery resulted in  $65.90 \pm 8.25\%$  editing, whereas Lipofectamine-CRISPRmax RNP delivery resulted in  $44.49 \pm 5.45\%$  editing. gDNA analysis from RNP-transfected cells showed 32.15% T->C conversion (Fig. 5C).

## DISCUSSION

In this study, we developed a reporter system for the efficient detection of gDNA editing by protein expression. Base editing of our rhodopsin model was confirmed by flow cytometry, western blotting, immunofluorescence microscopy, and DNA sequencing. We showed the proof-of-principle that LNP encapsulation of ABE results in increased editing efficiencies compared to traditional cationic polymer transfection. Further, we compared editing efficiency between plasmid delivery and RNP delivery of the ABE. Our reporter system is dependent on determining editing efficiency based on protein expression following treatment. However, editing efficiency based on these results does not directly correlate with editing efficiency based on gDNA sequencing. Summary of editing efficiencies can be found in Table 1.

The initial design of these experiments focused on sgRNA and ABE selection, which was dependent on the sequence of the mutant model. For these studies, the sgRNA and the ABE plasmid

were co-transfected into our reporter cell line using PEI as a suitable transfection agent. We selected candidate base editors based on the strongest available PAM that placed the adenine of interest at a position in the editing window amenable to deamination. Modifications to ABEs are continually being reported to optimize editing efficiency. The deaminase, which is responsible for chemically converting adenine to inosine, can be modified to act on different widths of the editing window. As shown in Fig. 2, ABE8e has an optimal editing window of position 3–12, whereas ABE7.10 is optimal at position 4–7. This is consistent with our findings that A6-sgRNA produced stronger editing than A3-sgRNA. Mutations on the edge of the editing window are less amendable to corrections, as shown by A3-sgRNA.

The xCas9 variant used here was engineered through phage-assisted continuous evolution to be compatible with NGN, GAT, and GAA PAMs [33]. This variant was evolved to broaden the range of PAM sequences that can be recognized. However, it showed limited on-target editing compared to wild-type SpCas9. This is consistent with our results, where we observed minimal on-target activity with xCas9 (Fig. 3B). SpCas9-NG, engineered from SpCas9 to recognize NGN PAMs, has previously been shown to exhibit the highest on-targeting activity among xCas9 and SpCas9 at a non-NGG site [34]. This is in agreement with our results in which we detected the highest editing efficiency with NG-ABE8e (Fig. 3B). ABE9 was developed to refine the editing window, with optimal editing at position A5, which explains why we detected editing (Fig. 3C) but not optimally at position A6 [35]. ABE9-SPRY was generated in-house for precision editing, not restricted by the NGG PAM. In our preliminary experiments (Fig. 3D), this novel base

**Table 1.** Comparison table of Rho Q344X editing with NG-ABE8e and A6-sgRNA.

ABE form	Transfection agent	Editing based on protein restoration (flow cytometry)	Editing based on protein restoration (western blotting)	Genomic DNA editing
Plasmid	Cationic polymer (PEI)	24% ± 5.8	N/A	30.7%
Plasmid	Lipid nanoparticle	65.9% ± 8.3	67.8 ± 12.9	42.4%
RNP	Cationic lipid (lipofectamine CRISPRmax)	44.5% ± 5.5	N/A	32.2%

editor was comparable to the editing efficiency of ABE8e and therefore would be interesting to explore in more detail.

We saw the highest efficiency with ABE8e (and NG-ABE8e) and A6-sgRNA because ABE8e has been shown to have the highest catalytic activity. Elevated catalytic activity associated with ABE8e has also been shown to increase bystander editing [36]. However, based on our sequencing results (Fig. 3E), there was limited bystander editing in our model. The bystander effects of base editing do remain a concern for clinical applications. To address these concerns, strategies are being employed to narrow the editing window, restricting the link between the Cas9 and deaminase, and limiting expression time in the cell [35, 37, 38]. For this reason, ribonucleoprotein delivery would be an excellent candidate to lower off-target mutations by limiting the duration of base editor expression.

One limitation of measuring base editing in this reporter system is the transfection efficiency of the plasmid base editor. To address this concern, we chose to include LNP transfection, which is known to be highly efficient with limited toxicity [39, 40]. Additionally, translation to a more biologically relevant *in vivo* model requires a viable transfection method. Previous findings using cationic polymer/lipid-based transfection agents (PEI, Lipofectamine, Turbofect) resulted in on-target editing, consistent with the 20% editing we found in our reporter models [6, 8, 19, 36]. Our findings show that LNP transfections led to a marked increase in editing efficiency (Fig. 4), supporting their potential as strong candidates for base editor delivery. The improved performance of LNPs was most likely due to increased transfection efficiency of LNPs and decreased toxicity [39–41]. When the ABE cargo is encapsulated, it is protected from enzymatic degradation and can be delivered to the cell by endocytosis. The pH of the endosome decreases as it matures, resulting in the protonation of the ionizable lipid and the release into the cytosol. The electrostatic interactions between the cationic ionizable lipid and the anionic endosomal membrane are thought to disrupt the membrane and allow for the escape of the cargo [42]. The majority of the components of the LNP are then recycled by the cell, whereas the PEI polymer is non-biodegradable, remains within the cells where it can cause cell toxicity [43].

In most standard LNP formulations, sodium acetate is used as the formulation buffer; however, in this study, we chose to co-encapsulate pDNA-ABE and sgRNA using a 300 mM Na-citrate buffer. This induces the formation of a bleb structure (Fig. 4A) that may suggest high loading and better protection toward the cargos, similar to what was previously observed with mRNA [25]. Based on size, PDI measurements of our particles, and encapsulation efficiency, encapsulation of the plasmid is comparable to that which was previously reported [25]. This formulation has also shown improved *in vivo* transfection properties following IV injection. Therefore, it would be interesting to explore if these findings are consistent following subretinal injections.

Optimization of editing of our reporter system primarily focused on plasmid delivery of the base editor. However, we have shown that RNP delivery is also a strong potential candidate (Fig. 5). RNPs have a fast onset of action and are then quickly degraded in the cell. This is advantageous over plasmid delivery, not only because it reduces the risk of random plasmid integration, but also because

the shorter time of Cas9 expression decreases the risk of off-target effects [44]. For our reporter model, cationic lipid transfection of the RNP showed higher editing than plasmid delivery. However, it is important to note that the editing efficiencies are reflective of both the different cargo and the distinct transfection methods, and therefore, the difference detected is not a direct result of the difference in cargo. Here, we have shown that RNP delivery by cationic polymer is a viable method of transfection and can produce editing efficiencies similar to plasmid transfection.

A future direction would be to explore the delivery of RNP encapsulated in LNPs to photoreceptor cells. A recent publication described RNP delivery to RPE cells *in vivo* using LNPs delivery [45]. This study showed increased editing efficiency using LNPs compared to lipofectamine transfection. This highlights the viability of LNP delivery of base editor cargo. However, encapsulation of base editor RNP into LNPs is not without its own challenges. The large size of the Cas9 endonuclease, its cationic surface charge, which limits its interaction with lipids used in LNP formulations, and the need to co-encapsulate the protein with sgRNA can result in a low level of encapsulation. Furthermore, preservation of endonuclease activity can be problematic due to the adverse conditions, such as low pH, often used in LNP formulations. Accordingly, efficient encapsulation of RNPs into LNPs requires optimization of lipid composition [46, 47]. Furthermore, translating the RNP-LNP delivery system into an *in vivo* model of rhodopsin-associated retinal degeneration presents additional challenges.

One recent publication explored direct delivery of the RNP to the retina *in vivo* using subretinal injection [48]. They saw localization of the RNP within photoreceptor cells, but also detected photoreceptor toxicity. These findings suggest that if LNPs can be engineered to effectively target photoreceptors, LNP encapsulation of RNP may help reduce such toxic effects.

The eye is a strong candidate for exploring LNP paired with ABE technology because it is immune privileged and has minimal systemic exposure [49]. The majority of IRDs are caused by the dysfunction of a protein within photoreceptors. *In vivo* base editing of the Q344X rhodopsin mutation model using LNPs is currently limited by targeting and delivery of the base editor cargo to photoreceptor cells. Recently, delivery and translation of LNP cargo to photoreceptors have been demonstrated [11–13]. However, delivery of a base editor and successful editing have yet to be shown. Lack of knowledge related to LNP endosomal uptake and release of the cargo into photoreceptor cells strongly limits our understanding of how to increase the uptake and translation of LNP cargo without causing toxicity. Whether the lack of photoreceptor transfection efficiency is due to limited cellular uptake or inefficiency of endosomal escape is not currently known. Future *in vivo* studies need to focus on optimization of the delivery of base editing cargo directly to photoreceptor cells.

Autosomal dominant RP linked to mutations in rhodopsin is highly prevalent, with over 150 mutations identified in patient populations [50]. The prevalence of these disease-causing mutations in rhodopsin highlights the need for effective therapies, of which we have laid the foundation in this study. We developed a reporter system that serves as a rapid and efficient platform for optimizing base editing. This reporter system, by itself, is not a definitive indicator of the strongest editing for future

implementation, but it demonstrates a viable and practical method of optimization by comparing sgRNAs, novel base editor variants, and delivery methods. We showed successful editing of the Q344X Rho mutation using ABE not only at a genomic level, but also at a protein expression level. Furthermore, this study highlights the requirements for optimization of an ABE system for the Q344X mutation. Importantly, this reporter system has a wide application for the optimization of base editing of other disease-associated mutations in rhodopsin. For the overall field of ocular gene therapy, this study shows both the successful implementation of base editing in a model of ocular disease, but also the fundamental difference that delivery vehicles and mode of cargo (plasmid vs. protein) can have on editing efficiency, underlining the need for further research in this field before these technologies can be translated into therapies. Finally, the *in vitro* reporter system developed here can be applied to the optimization of base editing of genetic mutations in non-ocular diseases.

## DATA AVAILABILITY

All the data produced in this study have been either included in the published paper or are accessible through the lead contact upon request.

## REFERENCES

- Hanany M, Rivolta C, Sharon D. Worldwide carrier frequency and genetic prevalence of autosomal recessive inherited retinal diseases. *Proc Natl Acad Sci USA*. 2020;117:2710–6.
- Hauswirth WW, Aleman TS, Kaushal S, Cideciyan AV, Schwartz SB, Wang L, et al. Treatment of leber congenital amaurosis due to RPE65 mutations by ocular subretinal injection of adeno-associated virus gene vector: short-term results of a phase I trial. *Hum Gene Ther*. 2008;19:979–90.
- Maguire AM, Simonelli F, Pierce EA, Pugh EN Jr., Mingozzi F, Bennicelli J, et al. Safety and efficacy of gene transfer for Leber's congenital amaurosis. *N Engl J Med*. 2008;358:2240–8.
- Bainbridge JW, Smith AJ, Barker SS, Robbie S, Henderson R, Balaggan K, et al. Effect of gene therapy on visual function in Leber's congenital amaurosis. *N Engl J Med*. 2008;358:2231–9.
- Huang TP, Newby GA, Liu DR. Precision genome editing using cytosine and adenine base editors in mammalian cells. *Nat Protoc*. 2021;16:1089–128.
- Choi EH, Suh S, Foik AT, Leinonen H, Newby GA, Gao XD, et al. *In vivo* base editing rescues cone photoreceptors in a mouse model of early-onset inherited retinal degeneration. *Nat Commun*. 2022;13:1830.
- Muller A, Sullivan J, Schwarzer W, Wang M, Park-Windhol C, Hasler PW, et al. High-efficiency base editing in the retina in primates and human tissues. *Nat Med*. 2025;31:490–501.
- Su J, She K, Song L, Jin X, Li R, Zhao Q, et al. *In vivo* base editing rescues photoreceptors in a mouse model of retinitis pigmentosa. *Mol Ther Nucleic Acids*. 2023;31:596–609.
- Peynshaert K, Devoldere J, De Smedt SC, Remaut K. *In vitro* and *ex vivo* models to study drug delivery barriers in the posterior segment of the eye. *Adv Drug Deliv Rev*. 2018;126:44–57.
- Chambers CZ, Soo GL, Engel AL, Glass IA, Birth Defects Research L, Frassetto A, et al. Lipid nanoparticle-mediated delivery of mRNA into the mouse and human retina and other ocular tissues. *Transl Vis Sci Technol*. 2024;13:7.
- Gautam M, Jozic A, Su GL, Herrera-Barrera M, Curtis A, Arrizabalaga S, et al. Lipid nanoparticles with PEG-variant surface modifications mediate genome editing in the mouse retina. *Nat Commun*. 2023;14:6468.
- Herrera-Barrera M, Ryals RC, Gautam M, Jozic A, Landry M, Korzun T, et al. Peptide-guided lipid nanoparticles deliver mRNA to the neural retina of rodents and nonhuman primates. *Sci Adv*. 2023;9:eadd4623.
- Eygeris Y, Henderson MI, Curtis AG, Jozic A, Stoddard J, Reynaga R, et al. Pre-formed vesicle approach to LNP manufacturing enhances retinal mRNA delivery. *Small*. 2024;20:e2400815.
- Hofmann KP, Lamb TD. Rhodopsin, light-sensor of vision. *Prog Retin Eye Res*. 2023;93:101116.
- Molday RS, Moritz OL. Photoreceptors at a glance. *J Cell Sci*. 2015;128:4039–45.
- Sung CH, Makino C, Baylor D, Nathans J. A rhodopsin gene mutation responsible for autosomal dominant retinitis pigmentosa results in a protein that is defective in localization to the photoreceptor outer segment. *J Neurosci*. 1994;14:5818–33.
- Concepcion F, Chen J. Q344ter mutation causes mislocalization of rhodopsin molecules that are catalytically active: a mouse model of Q344ter-induced retinal degeneration. *PLoS One*. 2010;5:e10904.
- Takita S, Jahan S, Imanishi S, Harikrishnan H, LePage D, Mann RJ, et al. Rhodopsin mislocalization drives ciliary dysregulation in a novel autosomal dominant retinitis pigmentosa knock-in mouse model. *FASEB J*. 2024;38:e23606.
- Du SW, Newby GA, Salom D, Gao F, Menezes CR, Suh S, et al. *In vivo* photoreceptor base editing ameliorates rhodopsin-E150K autosomal-recessive retinitis pigmentosa in mice. *Proc Natl Acad Sci USA*. 2024;121:e2416827121.
- Kaukonen M, McClements ME, MacLaren RE. CRISPR DNA base editing strategies for treating retinitis pigmentosa caused by mutations in rhodopsin. *Genes*. 2022;13:1327.
- Choi H, Andersen JP, Molday RS. Expression and functional characterization of missense mutations in ATP8A2 linked to severe neurological disorders. *Hum Mutat*. 2019;40:2353–64.
- Garces F, Jiang K, Molday LL, Stohr H, Weber BH, Lyons CJ, et al. Correlating the expression and functional activity of ABCA4 disease variants with the phenotype of patients with Stargardt disease. *Invest Ophthalmol Vis Sci*. 2018;59:2305–15.
- Clement K, Rees H, Canver MC, Gehrke JM, Farouni R, Hsu JY, et al. CRISPResso2 provides accurate and rapid genome editing sequence analysis. *Nat Biotechnol*. 2019;37:224–6.
- Kulkarni JA, Witzigmann D, Leung J, van der Meel R, Zaifman J, Darjuan MM, et al. Fusion-dependent formation of lipid nanoparticles containing macromolecular payloads. *Nanoscale*. 2019;11:9023–31.
- Cheng MHY, Leung J, Zhang Y, Strong C, Basha G, Momeni A, et al. Induction of Bleb structures in lipid nanoparticle formulations of mRNA leads to improved transfection potency. *Adv Mater*. 2023;35:e2303370.
- Mayuranathan T, Newby GA, Feng R, Yao Y, Mayberry KD, Lazzarotto CR, et al. Potent and uniform fetal hemoglobin induction via base editing. *Nat Genet*. 2023;55:1210–20.
- Molday RS. Monoclonal antibodies to rhodopsin and other proteins of rod outer segments. *Prog Retinal Res*. 1988;8:173–209.
- Doi T, Molday RS, Khorana HG. Role of the intradiscal domain in rhodopsin assembly and function. *Proc Natl Acad Sci USA*. 1990;87:4991–5.
- Lv H, Zhang S, Wang B, Cui S, Yan J. Toxicity of cationic lipids and cationic polymers in gene delivery. *J Control Release*. 2006;114:100–9.
- Jain S, Kumar S, Agrawal AK, Thanki K, Banerjee UC. Enhanced transfection efficiency and reduced cytotoxicity of novel lipid-polymer hybrid nanoplexes. *Mol Pharm*. 2013;10:2416–25.
- Cullis PR, Felgner PL. The 60-year evolution of lipid nanoparticles for nucleic acid delivery. *Nat Rev Drug Discov*. 2024;23:709–22.
- Akinc A, Maier MA, Manoharan M, Fitzgerald K, Jayaraman M, Barros S, et al. The Onpatro story and the clinical translation of nanomedicines containing nucleic acid-based drugs. *Nat Nanotechnol*. 2019;14:1084–7.
- Hu JH, Miller SM, Geurts MH, Tang W, Chen L, Sun N, et al. Evolved Cas9 variants with broad PAM compatibility and high DNA specificity. *Nature*. 2018;556:57–63.
- Nishimasu H, Shi X, Ishiguro S, Gao L, Hirano S, Okazaki S, et al. Engineered CRISPR-Cas9 nuclease with expanded targeting space. *Science*. 2018;361:1259–62.
- Chen L, Zhang S, Xue N, Hong M, Zhang X, Zhang D, et al. Engineering a precise adenine base editor with minimal bystander editing. *Nat Chem Biol*. 2023;19:101–10.
- Tu T, Song Z, Liu X, Wang S, He X, Xi H, et al. A precise and efficient adenine base editor. *Mol Ther*. 2022;30:2933–41.
- Gaudelli NM, Komor AC, Rees HA, Packer MS, Badran AH, Bryson DI, et al. Programmable base editing of A•T to G•C in genomic DNA without DNA cleavage. *Nature*. 2017;551:464–71.
- Lin Y, Wagner E, Lachelt U. Non-viral delivery of the CRISPR/Cas system: DNA versus RNA versus RNP. *Biomater Sci*. 2022;10:1166–92.
- Kafetzis KN, Papalamprou N, McNulty E, Thong KX, Sato Y, Mironov A, et al. The effect of cryoprotectants and storage conditions on the transfection efficiency, stability, and safety of lipid-based nanoparticles for mRNA and DNA delivery. *Adv Health Mater*. 2023;12:e2203022.
- Quagliarini E, Wang J, Renzi S, Cui L, Digiacoio L, Ferri G, et al. Mechanistic insights into the superior DNA delivery efficiency of multicomponent lipid nanoparticles: an *in vitro* and *in vivo* study. *ACS Appl Mater Interfaces*. 2022;14:56666–77.
- Kunath K, von Harpe A, Fischer D, Petersen H, Bickel U, Voigt K, et al. Low-molecular-weight polyethylenimine as a non-viral vector for DNA delivery: comparison of physicochemical properties, transfection efficiency and *in vivo* distribution with high-molecular-weight polyethylenimine. *J Control Release*. 2003;89:113–25.
- Semple SC, Akinc A, Chen J, Sandhu AP, Mui BL, Cho CK, et al. Rational design of cationic lipids for siRNA delivery. *Nat Biotechnol*. 2010;28:172–6.

43. Wen Y, Pan S, Luo X, Zhang X, Zhang W, Feng M. A biodegradable low molecular weight polyethylenimine derivative as low toxicity and efficient gene vector. *Bioconj Chem*. 2009;20:322–32.
44. Ono R, Yasuhiko Y, Aisaki KI, Kitajima S, Kanno J, Hirabayashi Y. Exosome-mediated horizontal gene transfer occurs in double-strand break repair during genome editing. *Commun Biol*. 2019;2:57.
45. Holubowicz R, Du SW, Felgner J, Smidak R, Choi EH, Palczewska G, et al. Safer and efficient base editing and prime editing via ribonucleoproteins delivered through optimized lipid-nanoparticle formulations. *Nat Biomed Eng*. 2025;9:57–78.
46. Im SH, Jang M, Park JH, Chung HJ. Finely tuned ionizable lipid nanoparticles for CRISPR/Cas9 ribonucleoprotein delivery and gene editing. *J Nanobiotechnol*. 2024;22:175.
47. Walther J, Porenta D, Wilbie D, Seinen C, Benne N, Yang Q, et al. Comparative analysis of lipid Nanoparticle-Mediated delivery of CRISPR-Cas9 RNP versus mRNA/sgRNA for gene editing in vitro and in vivo. *Eur J Pharm Biopharm*. 2024;196:114207.
48. Pulman J, Botto C, Malki H, Ren D, Oudin P, De Cian A, et al. Direct delivery of Cas9 or base editor protein and guide RNA complex enables genome editing in the retina. *Mol Ther Nucleic Acids*. 2024;35:102349.
49. Ghoraba HH, Akhavanrezayat A, Karaca I, Yavari N, Lajevardi S, Hwang J, et al. Ocular gene therapy: a literature review with special focus on immune and inflammatory responses. *Clin Ophthalmol*. 2022;16:1753–71.
50. Athanasiou D, Aguila M, Bellingham J, Li W, McCulley C, Reeves PJ, et al. The molecular and cellular basis of rhodopsin retinitis pigmentosa reveals potential strategies for therapy. *Prog Retin Eye Res*. 2018;62:1–23.

## ACKNOWLEDGEMENTS

We thank Dr. Jonathen Yen for the NG-ABE8e ribonucleoprotein expression plasmid and Dr. Orson Moritz for the murine rhodopsin cDNA. Ryan Zhu assisted in RNP purification. Cryo-TEM data was collected at the High-Resolution Macromolecular Electron Microscopy (HRMEM) facility at UBC supported by the Canadian Foundation of Innovation and the British Columbia Knowledge Development Fund.

## AUTHOR CONTRIBUTIONS

RSM and VACP conceived the overall project. VACP, MHYC, YZ, TC, TM, JL designed the experiments, acquired the data and along with RSM, CJDR, and PRC analyzed and

interpreted the data. RSM, CJDR and PRC supervised the study and provided resources. VACP and RSM wrote the original draft of the manuscript. All authors reviewed, edited and approved the manuscript.

## FUNDING

This study was supported by the Canadian Institutes of Health Research (CIHR) grant 175118 and an unrestricted UBC research grant to RSM and CIHR grant 148469 to PRC. MHYC was supported by the NanoMedicines Innovation Network postdoctoral fellowship in gene therapy and the CIHR Research Excellence, Diversity, and Independence (REDI) Early Career Transition Award. Y.Z. (FBD 193487) and JL was supported by a Frederick Banting and Charles Best Canada Graduate Scholarships Doctoral Award. VACP, YZ, and TM were awarded NanoMedicines Innovation Network (NMNI) graduate awards.

## COMPETING INTERESTS

PRC has financial interests in Acuitas Therapeutics, Mesentech, and NanoVation Therapeutics. The other authors declare no competing interests.

## ADDITIONAL INFORMATION

**Supplementary information** The online version contains supplementary material available at <https://doi.org/10.1038/s41434-025-00584-z>.

**Correspondence** and requests for materials should be addressed to Robert S. Molday.

**Reprints and permission information** is available at <http://www.nature.com/reprints>

**Publisher's note** Springer Nature remains neutral with regard to jurisdictional claims in published maps and institutional affiliations.

Springer Nature or its licensor (e.g. a society or other partner) holds exclusive rights to this article under a publishing agreement with the author(s) or other rightsholder(s); author self-archiving of the accepted manuscript version of this article is solely governed by the terms of such publishing agreement and applicable law.